ChemComm

COMMUNICATION

View Article Online
View Journal | View Issue

Cite this: *Chem. Commun.*, 2024, **60**, 3031

Received 3rd November 2023,
Accepted 4th January 2024

DOI: 10.1039/d3cc05419e

rsc.li/chemcomm

A non-peptide-based fluorescent probe capable of sensitively visualizing asparagine endopeptidase†

Kang Li,[a] Yanxian Hou,[a] Jinliang Han,[a] Chengyuan Lv,[a] Wenkai Liu,[a] Jianjun Du,[a] Wen Sun,[a] Jiangli Fan *[ab] and Xiaojun Peng[a]

The non-peptide-based fluorescent probe QMC11 is capable of specifically targeting asparagine endopeptidase (AEP) and imaging cellular endogenous AEP. The motion of the probe can be restricted by AEP to activate fluorescence while keeping a low background signal.

Asparagine endopeptidase (AEP) is a member of the C13 cysteine protease family, predominantly found in cellular lysosomes.[1] It specifically cleaves peptide bonds in the carboxyl terminus of aspartic acid (Asn) or aspartic acid (Asp) residues. The abnormal upregulation of AEP, compared with other biomarkers of Alzheimer's disease (AD) such as amyloid-β (Aβ),[2,3] β-secretase (BACE1), tau protein, monoamine oxidases (MAOs), and methionine sulfoxide reductase (Msrs), is present in the early stage of the entire pathological process.[4,5] At the same time, the upregulation of AEP leads to accumulation of Aβ protein, cleavage of SET (protein phosphatase 2A inhibitor 2) and abnormal aggregation of Tau, all of which contribute to the progression of both elderly and AD patients.[6–11] This cascade effect is not seen with other biomarkers. Thus, the elevated AEP activation is considered an important marker in the regulation of pathological pathways and pre-monitoring in Alzheimer's disease.[12,13]

In recent years, various methods, such as mass spectrometry,[14] immunoproteomic analysis,[15] and magnetic resonance imaging (MRI),[16] have been employed to detect AEP. However, these methods possess certain drawbacks including their complex technology, high costs, and the requirement of large instruments and equipment. Comparatively, fluorescence imaging exhibits several advantages such as non-invasiveness, real-time monitoring, and high sensitivity. Due to its specificity for substrates containing aspartate (Asp), AEP can cut certain specific polypeptide sequences.[17] Consequently, a few fluorescent probes targeting AEP have been designed based on peptide substrates containing aspartic acid (Asp).[18–23] But the synthesis and purification of substrates based on proteins or peptides entail multiple steps, thereby increasing the preparation difficulties of the probes.[21,22] Also, some of them could not only be cleaved by AEP, but also by caspases, which means that the specificity to AEP was weak. To overcome these limitations, alternative strategies for AEP detection should be explored to avoid introducing peptide chains.

We chose the fluorophore sulfonate-substituted quinoline-malononitrile (QM-SO_3) as the fluorescence reporting unit,[24] in which the oxygen atom in the fluorophore **DCM** was replaced by a nitrogen atom to overcome the quenching effect and a sulfonate group was introduced to enhance the water solubility. **C11** has been screened as a non-toxic δ-secretase (AEP) inhibitor through high throughput, specifically targeting AEP without affecting other related cysteine proteases. Additionally, it was found that the presence of an amino group on **C11** did not impact the binding to AEP.[25] Therefore, the amino group could serve as the active site for attaching the fluorophore. Combining these ideas, we herein presented **QMC11**, a new small molecule fluorescent probe (Fig. 1A) by connecting QMN3 and **C11** through click reaction. **QMC11** was not fluorescent in the physiological environment unless it specifically bound to AEP. The binding mode was mainly hydrogen bonding, and the binding sites included benzoxadiazole of **C11** and the sulfonic acid group part. The binding restricted the molecular rotation and conformational change, thereby turning on the fluorescence. The probe molecule exhibited high SNR (~35-fold) and greater specificity for AEP compared to other substances. As illustrated in Fig. 1B, the targeted portion of **QMC11** contained a morpholine ring, which facilitated its arrival to the lysosomal region, where it combined with the highly expressed AEP to enable the fluorescence signal to be turned on.

The details of the synthetic procedure are presented in Scheme S1 (ESI†). Key intermediates and the final product

[a] *State Key Laboratory of Fine Chemicals, Frontiers Science Centre for Smart Materials Oriented Chemical Engineering, Dalian University of Technology, Dalian 116024, China. E-mail: fanjl@dlut.edu.cn*
[b] *Ningbo Institute of Dalian University of Technology, Ningbo 315016, China*

† Electronic supplementary information (ESI) available. See DOI: https://doi.org/10.1039/d3cc05419e

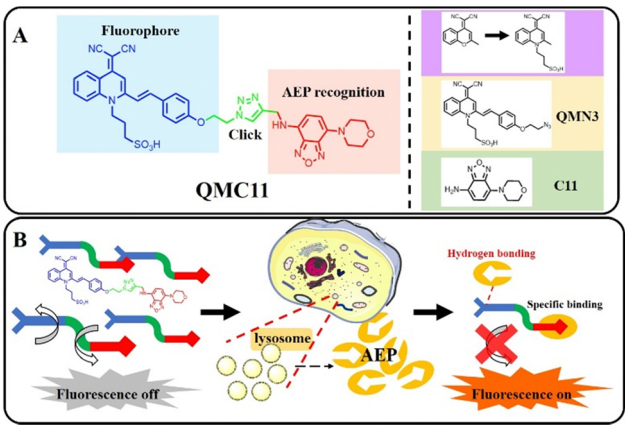

Fig. 1 (A) The structure and design principle of **QMC11**. (B) Specific identification of the AEP mechanism.

were characterized with ^{1}H-NMR, ^{13}C-NMR, and ESI-HRMS (Fig. S11–S13, ESI†).

Firstly, the fluorescence properties of **QMC11** in different solvent systems were conducted. **QMC11** demonstrated good solubility in water, and it was not emissive in aqueous solution, ethanol, or tetrahydrofuran (Fig. 2A and Fig. S1A, ESI†). However, in the water–glycerol system, the fluorescence at 550 nm was continuously enhanced as the volume fraction of glycerol in the mixed solvent reached 99% (Fig. S1B, ESI†). These observations indicated a correlation between **QMC11** and the viscosity of the system. To determine whether AEP is sufficient to turn on fluorescence by binding the inhibitor (**C11**), QMN3, which lacks the target group **C11** (Fig. 1), was synthesized. It also remained non-emissive in aqueous solution, ethanol, and tetrahydrofuran and responded to the viscosity (Fig. S2, ESI†). It was reported that the maximal activity of AEP was at pH 4–6 under normal assay conditions, and the enzyme was irreversibly denatured at pH 7 and above.[26] To determine the stability of **QMC11** over a specific pH range, the effects of pH on **QMC11** were tested using a glycerin–PBS solvent system (glycerin : PBS = 9 : 1) and the fluorescence behavior was investigated at pH levels ranging from 3 to 8 (Fig. 2B). It was observed that the fluorescence signal of **QMC11** was minimally affected by pH, indicating its good stability.

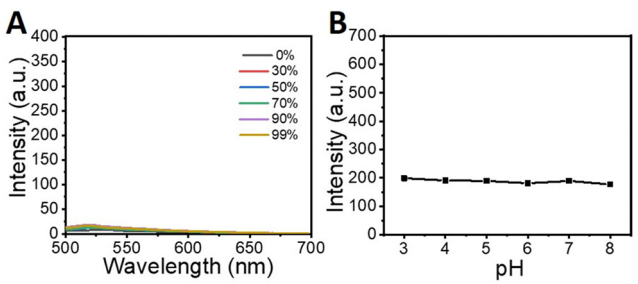

Fig. 2 *In vitro* tests of **QMC11**, λ_{ex}: 478 nm. (A) Fluorescence spectroscopy of **QMC11** (10 μM) in a mixture of water–ethanol with different ethanol fractions. (B) Fluorescence intensity of **QMC11** (5 μM) at different pH 3–8 (glycerin–PBS system).

The binding behavior of **QMC11** was investigated by performing an enzyme binding experiment *in vitro* using the buffer (pH = 4.5). Upon association with AEP, a significant fluorescence enhancement was observed from **QMC11**, as shown in Fig. 3A. It took approximately 90 minutes for the fluorescence to reach a plateau, as shown in Fig. 3B. In contrast, Fig. S3 (ESI†) illustrated that QMN3, without **C11**, did not produce a fluorescent signal upon the addition of AEP. Additionally, it was observed that with the increase of the AEP concentration, the fluorescence intensity of **QMC11** gradually increased (Fig. 3C). This might be due to the fact that as **QMC11** binds to AEP, while the AEP concentration increased, their

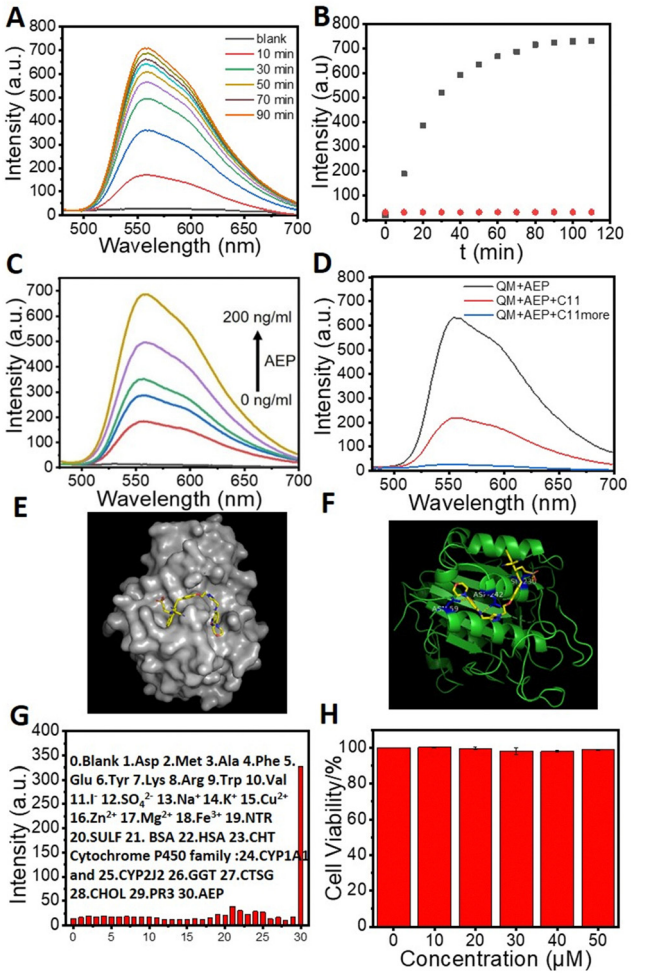

Fig. 3 Response tests of **QMC11** (20 μM except Fig. 3G, λ_{ex}: 478 nm). (A) Fluorescence spectra of **QMC11** with incubation with AEP (200 ng mL^{-1}). (B) Kinetics of **QMC11** (black) and QMN3 (20 μM; red) fluorescence response to AEP. (C) The fluorescence spectroscopy of various concentrations of AEP (0–200 ng mL^{-1}) incubated with **QMC11** for 90 min. (D) Inhibition of fluorescence response of **QMC11** and AEP by addition of **C11** (20 μM). (E) Simulated docking model of **QMC11** with AEP. (F) The action sites in the simulation docking model. (G) Selectivity of **QMC11** (10 μM) toward different analytes (0–30: blank, Asp, Met, Ala, Phe, Glu, Tyr, Lys, Arg, Trp, Val, I^-, SO_4^{2-}, Na^+, K^+, Cu^{2+}, Zn^{2+}, Mg^{2+}, Fe^{3+}, NTR, SULF, BSA, HAS, CHT Cytochrome P450 family, CYP1A1 and CYP2J2, GGT, CTSG, CHOL, PR3, AEP). Values are means ± SD (n = 3). (H) Cytotoxicity test of **QMC11** (MTT).

conformational change and rotation were more restricted, resulting in enhanced fluorescence. To confirm the specific binding of the inhibitor part to AEP, we further added the mother liquor of inhibitor **C11** to the incubated probe molecule and observed a gradual weakening and eventual disappearance of the fluorescence signal (Fig. 3D). To evaluate the specificity of **QMC11** for AEP, potentially competitive species including amino acids, anions, cations and protein macromolecules were tested. Fig. 3G illustrates that **QMC11** did not exhibit any fluorescence response to these species, indicating its fine specificity for AEP.

The docking study showed that the five-membered ring portion of benzoxadiazole of **C11** would nicely bind to amino acid residue regions such as ASN-159 and ASP-242 *via* hydrogen bonding. Surprisingly, additional hydrogen bonds were also found between the sulfonic acid group portion of **QMC11** and ASN-236 (Fig. 3E and F). Moreover, the binding energy of **QMC11** and AEP was -8.3 kcal mol^{-1}, indicating a strong affinity and potential for stable combination. This suggested that AEP had the ability to restrict the motion of the probe molecule, such as rotation and conformational change.

Based on the above properties we explored the application of **QMC11** in living cells. Prior to bioimaging, the cell cytotoxicity of **QMC11** was assessed using an MTT assay. We chose C6 cells (rat glioma cells), which express a significant level of AEP.[27] As shown in Fig. 3H and Fig. S4 (ESI†), when incubated with **QMC11** at the concentration of 10, 20, 40, 80 or 120 μM for 24 h, the viability of C6 cells was 99.2%, 99.7%, 98.2%, 97.8%, and 98.8%, respectively. Meanwhile, when incubated with QMN3 for 24 h, 96.0%, 94.5%, 93.0%, 93.1%, and 95.2% of C6 cells survived, respectively. The results indicated that over 95.0% of C6 cells retained viability in the presence of 40 μM of **QMC11** over 24 h, demonstrating its low cytotoxicity and safety for cell imaging. Next, in order to determine whether **QMC11** can enter cells and combine with cellular AEP, we incubated this probe with C6 cells. Meanwhile, we also incubated the control probe QMN3 alone with C6 cells. After a 1-h incubation, **QMC11** permeated into the cytoplasm and emitted fluorescence (Fig. 4A), indicating that rotation of **QMC11** was inhibited due to AEP specifically binding to **C11**. In contrast, C6 cells incubated with QMN3 showed little fluorescence (Fig. S5, ESI†). Moreover, when C6 cells were pre-treated with **C11** (40 μM), the fluorescence of **QMC11** was suppressed (Fig. 4B). These results were consistent with *in vitro* experiments, which showed that the specific binding of **QMC11** and AEP was indeed due to the **C11** part. In order to determine whether viscosity has an effect on **QMC11** in cells, we incubated **QMC11** with 4T1 cells (mouse breast cancer cell 4T1, no AEP expression[27]) for 1 h. Fortunately, no fluorescent signal appeared, indicating that the viscosity of cancer cells had no effect on **QMC11** (Fig. S8, ESI†). Thus, it could be concluded that **QMC11** was able to combine with cellular AEP and emitted fluorescence.

We verified the AEP expression levels of C6 and U251 through Western Blot experiments, indicating that C6 would overexpress AEP (Fig. S7, ESI†). In addition, we confirmed the high intracellular expression of AEP by immunofluorescence

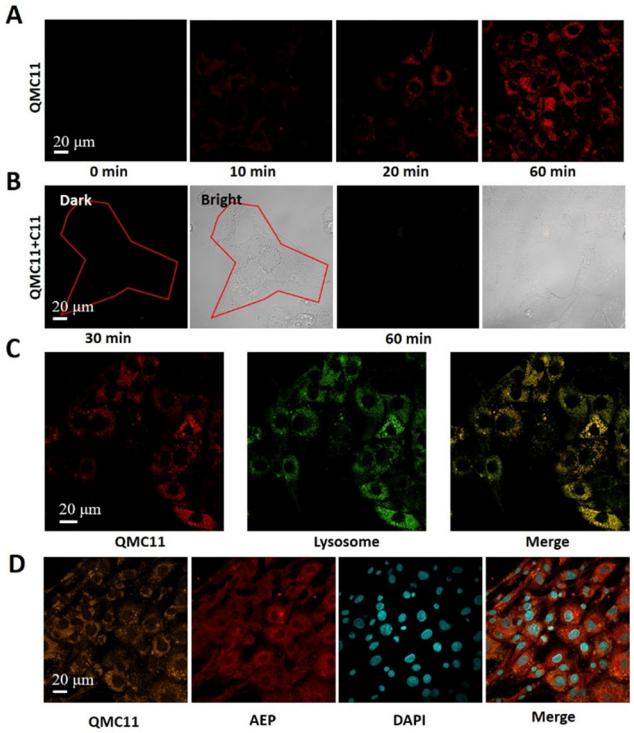

Fig. 4 Cellular uptake of **QMC11** (40 μM) and its fluorescence intensity in C6 cells. (λ_{ex}: 478 nm, λ_{em}: 500–580 nm, scale bars: 20 μm). (A) Image of C6 cells incubated with **QMC11** for 1 h. (B) 40 μM **C11** was added to inhibit AEP (30 min and 60 min). (C) **QMC11** was co-localized with Lysotracker Red in C6 cells (Pearson correlation coefficient: 0.905) (Lysotracker Red: λ_{ex}: 579 nm, λ_{em}: 600–650 nm, scale bars: 20 μm). (D) Uptake of **QMC11** into the cytoplasm after incubation with C6 cells for 1 h. Immunofluorescence images of AEP were co-localized with **QMC11** in the cytoplasm. (AEP: λ_{ex}: 650 nm, λ_{em}: 660–720 nm, scale bars: 20 μm; DAPI: λ_{ex}: 359 nm, λ_{em}: 420–480 nm, scale bars: 20 μm).

staining, further revealing the relationship between **QMC11** and AEP in C6 cells. Fluorescence signals in the orange, red, and blue channels were observed in Fig. 4D. We found that **QMC11** (orange) was co-localized with AEP (red) in the cytoplasm of C6 cells. Given that cellular AEP becomes activated in the acidic environment of lysosomes,[28] **QMC11** must at least enter lysosomes to combine with AEP. To investigate the subcellular localization of **QMC11**, we incubated C6 cells with **QMC11** for 1 h and employed a lysosome-targeted fluorescent dye Lysotracker Red. By imaging the red and green channels, we found that the red channel image overlapped well with the green channel image, indicating that the probe got into lysosomes where it played a significant role (Fig. 4C). Simultaneously, we found that it exhibits poor colocalization with mitochondria and the endoplasmic reticulum (Fig. S9 and S10, ESI†). Therefore, based on the endogenous AEP activity, **QMC11** could real-time monitor AEP.

In summary, a new small molecule fluorescent probe **QMC11** was designed by connecting a water-soluble fluorophore and a non-toxic AEP inhibitor **C11** through click reaction. **QMC11** did not exhibit fluorescence in the physiological environment, but was selectively turned on by AEP with high

sensitivity. Importantly, **QMC11** could stain lysosomal AEP in live cells. In contrast to other probes that require numerous steps for the synthesis and purification of substrates relying on proteins or peptides, **QMC11** provided a simpler synthesis process and avoided the interference of caspases. We thought it might be a different way to identify early abnormal biomarkers of AD.

This work was financially supported by the National Natural Science Foundation of China (21925802, 22338005), Liaoning Binhai Laboratory (LBLB-2023-03) and the Fundamental Research Funds for the Central Universities (DUT22LAB601).

Conflicts of interest

There are no conflicts to declare.

Notes and references

1 L. Calugi, E. Lenci, F. Bianchini, A. Contini and A. Trabocchi, *Bioorg. Med. Chem.*, 2022, **63**, 116746.
2 X. Wang, A. Iyaswamy, D. Xu, S. Krishnamoorthi, S. G. Sreenivasmurthy, Y. Yang, Y. Li, C. Chen, M. Li, H.-W. Li and M. S. Wong, *ACS Appl. Mater. Interfaces*, 2022, **15**, 39–47.
3 J. An, P. Verwilst, H. Aziz, J. Shin, S. Lim, I. Kim, Y. K. Kim and J. S. Kim, *Bioact. Mater.*, 2022, **13**, 239–248.
4 S. Ma, G. Chen, J. Xu, Y. Liu, G. Li, T. Chen, Y. Li and T. D. James, *Coord. Chem. Rev.*, 2021, **427**, 213553.
5 R. Ni, Z. Chen, X. L. Deán-Ben, F. F. Voigt, D. Kirschenbaum, G. Shi, A. Villois, Q. Zhou, A. Crimi, P. Arosio, R. M. Nitsch, K. P. R. Nilsson, A. Aguzzi, F. Helmchen, J. Klohs and D. Razansky, *Nat. Biomed. Eng.*, 2022, **6**, 1031–1044.
6 C. Kaether, C. Haass and H. Steiner, *Neurodegener. Dis.*, 2006, **3**, 275–283.
7 W. A. Campbell, M. L. Reed, J. Strahle, M. S. Wolfe and W. Xia, *J. Neurochem.*, 2003, **85**, 1563–1574.
8 K. Blennow, C. Chen, C. Cicognola, K. R. Wildsmith, P. T. Manser, S. M. S. Bohorquez, Z. Zhang, B. Xie, J. Peng, O. Hansson, H. Kvartsberg, E. Portelius, H. Zetterberg, T. Lashley, G. Brinkmalm, G. A. Kerchner, R. M. Weimer, K. Ye and K. Hoglund, *Brain*, 2020, **143**, 650–660.
9 G. Basurto-Islas, I. Grundke-Iqbal, Y. C. Tung, F. Liu and K. Iqbal, *J. Biol. Chem.*, 2013, **288**, 17495–17507.
10 C. M. Yates, John Buttenvorth, T. Mara C. Tennant and A. Gordon, *J. Neurochem.*, 1990, **55**, 1624–1630.
11 K. Wang, H. Gao, Y. Zhang, H. Yan, J. Si, X. Mi, S. Xia, X. Feng, D. Liu, D. Kong, T. Wang and D. Ding, *Adv. Mater.*, 2022, **34**, 2106994.
12 M. Song, *Int. J. Mol. Sci.*, 2022, **23**, 10223–10236.
13 P. Griffin, L. Apostolova, B. C. Dickerson, G. Rabinovici, S. Salloway, K. Brandt, J. Masdeu, D. Hammers, S. Raghuram, S. Hall and M. C. Carrillo, *Alzheimer's Dementia*, 2023, **19**, S126–S131.
14 A. Dutta, D. Potier, M. Walker, O. Gray and A. D. Whetton, *Oncotarget*, 2016, **7**, 70822–70831.
15 J.-W. Ju, H.-N. Joo, M.-R. Lee, S.-H. Cho, H.-I. Cheun, J.-Y. Kim, Y.-H. Lee, K.-J. Lee, W.-M. Sohn, D.-M. Kim, I.-C. Kim, B. C. Park and T.-S. Kim, *Proteomics*, 2009, **9**, 3066–3078.
16 Y. Yuan, S. Ge, H. Sun, X. Dong and H. Zhao, *ACS Nano*, 2015, **9**, 5117–5124.
17 M. Poreba, R. Solberg, W. Rut, N. N. Lunde, P. Kasperkiewicz, S. J. Snipas, M. Mihelic, D. Turk, B. Turk, G. S. Salvesen and M. Drag, *Cell Chem. Biol.*, 2016, **23**, 1023–1035.
18 X. Li, Q. Liu, S. Ye, S. Wang, K. Li, G. Lv, Y. Peng, L. Qiu and J. Lin, *Chem. Biol. Drug Des.*, 2019, **94**, 1494–1503.
19 J. Lee and M. Bogyo, *ACS Chem. Biol.*, 2010, **5**, 233–243.
20 J. A. Hong, N. E. Choi, Y. K. La, H. Y. Nam, J. Seo and J. Lee, *Org. Biomol. Chem.*, 2017, **15**, 8018–8022.
21 L. E. Edgington, M. Verdoes, A. Ortega, N. P. Withana, J. Lee, S. Syed, M. H. Bachmann, G. Blum and M. Bogyo, *J. Am. Chem. Soc.*, 2013, **135**, 174–182.
22 Y. Zhao, Z. Hai, H. Wang, L. Su and G. Liang, *Anal. Chem.*, 2018, **90**, 8732–8735.
23 K. B. Sexton, M. D. Witte, G. Blum and M. Bogyo, *Bioorg. Med. Chem. Lett.*, 2007, **17**, 649–653.
24 W. Fu, C. Yan, Z. Guo, J. Zhang, H. Zhang, H. Tian and W. H. Zhu, *J. Am. Chem. Soc.*, 2019, **141**, 3171–3177.
25 Z. Zhang, O. Obianyo, E. Dall, Y. Du, H. Fu, X. Liu, S. S. Kang, M. Song, S. P. Yu, C. Cabrele, M. Schubert, X. Li, J. Z. Wang, H. Brandstetter and K. Ye, *Nat. Commun.*, 2017, **8**, 14740.
26 J.-M. Chen, P. M. Dando, N. D. Rawlings, M. A. Brown, N. E. Young, R. A. Stevens, E. Hewitt, C. Watts and A. J. Barrett, *J. Biol. Chem.*, 1997, **272**, 8090–8098.
27 S. Ruan, C. Hu, X. Tang, X. Cun, W. Xiao, K. Shi, Q. He and H. Gao, *ACS Nano*, 2016, **10**, 10086–10098.
28 E. Dall and H. Brandstetter, *Biochimie*, 2016, **122**, 126–150.

